Ageostrophic, anticyclonic instability of a geostrophic, barotropic boundary current

James C. McWilliams and M. Jeroen Molemaker
Institute of Geophysics and Planetary Physics, University of California, Los Angeles, California 90095-1567

Irad Yavneh
Department of Computer Sciene, Technion, Haifa 32000, Israel

After having previously demonstrated the occurrence of ageostrophic, anticyclonic instability (AAI) for several other steady flows, in this paper we further test the hypothesis that rotating, stably stratified, shear flows are generally subject to AAI at finite Rossby (Ro) and Froude (Fr) numbers by calculating the inviscid, incompressible normal modes of a geostrophic, barotropic boundary current that vanishes toward the interior of the domain. We focus on a background current profile with no inflection point and nonvanishing absolute vorticity to exclude other known instability types. The hypothesis is again confirmed. The instability occurs for finite Ro only in an anticyclonic background flow. Its modal growth rate steeply decreases (approximately inverse exponentially, $\sim e^{-c/\text{Ro}}$) as Ro$\rightarrow$0. The downstream phase velocity of the unstable mode lies within the speed range for the background current, so the eigenmode has a near-critical layer within the zone of strong background shear. Its unstable eigenmode has an aspect ratio of downstream and vertical wave numbers, l/m, on the order of the ratio of the Coriolis and Brünt-Väisällä frequencies (as is typical for rotating, stratified flows). The maximum growth rate is independent of Fr for small Fr (the usual geophysical regime), and it decreases with large Fr, disappearing when there is no stratification. The eigenmode has a weakly decaying, oscillatory, interior far-field structure similar to an inertia-gravity wave. This supports the interpretation that the modal instability arises through the coalescence (i.e., resonance) of two stable normal-mode branches, one associated with the background shear flow and the other an inertia-gravity or Kelvin wave mode. © *2004 American Institute of Physics.*
[DOI: 10.1063/1.1785132]

I. INTRODUCTION

Under the combined influences of stable density stratification and planetary rotation, large-scale currents and winds typically are constrained by a diagnostic force balance that is the combination of hydrostatic balance in the vertical direction (parallel to gravity) and either geostrophic or gradient-wind balance in the horizontal plane. This regime, often called quasigeostrophy in its asymptotic limit, is characterized by small Rossby and Froude numbers,

$$\text{Ro} = V_o/fL \ll 1, \quad \text{Fr} = V_o/NH \ll 1, \tag{1}$$

and weak vertical velocity,

$$W_o \ll V_o H/L. \tag{2}$$

Here V_o is a characteristic horizontal velocity magnitude, H and L are vertical and horizontal lengths, f is the Coriolis frequency, and N is the Brünt-Väisällä (or buoyancy) frequency. Alternatively, when Ro and Fr are large (i.e., rotational and stratification influences are weak), the vertical motions are strong, and the fluid accelerations are much larger due to the appreciably unbalanced forces. In atmospheric and oceanic flows, the quasigeostrophic approximation is often apt for planetary- and large-scale flows, while small-scale flows are usually significantly unbalanced. Here we are interested in the transitional regime between these extremes,

which occurs on the so-called atmospheric mesoscale (with L between about 1 and 1000 km) and oceanic mesoscale and "submesoscale" (with L between about 10 m and 100 km).

In particular we are interested in dynamical mechanisms for escaping the prevalent constraint of diagnostic force balance.[1] Inertia-gravity waves, of course, avoid this constraint, but they are generally understood to be weakly coupled to balanced flows with significant advection. Several advective mechanisms for escape are well known, and they are often characterized by an instability of a stationary state:[2] gravitational instability for $N < 0$; centrifugal or inertial instability for absolute vertical vorticity, $A = f + \zeta$, changing sign (with ζ the vertical relative vorticity); and Kelvin–Helmholtz instability for Fr above a critical value > 1. We have recently shown that another mechanism, which we call anticyclonic, ageostrophic instability (AAI), arises in several canonical shear flows. These include elliptical flow,[3] Taylor–Couette flow,[4,5] and baroclinic flow.[6] AAI arises for anticyclonic flows with moderate Rossby number ($0 < A/f < 1$) and significant stratification (Fr < 1). All of these flows have fully three-dimensional unstable eigenmodes. Furthermore, for flows in a shallow water layer, there is an analogous two-dimensional, ageostrophic instability for parallel, anticyclonic flows.[7–9]

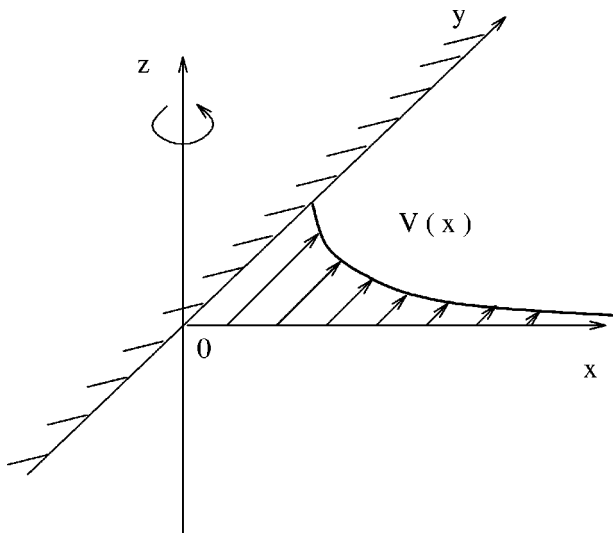In all these examples, the identified ageostrophic insta-

FIG. 1. The background current for the eigenvalue calculations: a barotropic boundary current that decays in the cross-stream direction in a uniformly stratified and rotating environment.

bility occurs in and beyond the parametric neighborhood of a singularity in the time integrability of the so-called balance equations that embody a fully diagnostic force balance;[10] the circumstances for this singularity are characterized by the occurrence of any of the conditions $N^2 < 0$, $A/f < 0$, or $A/f - |S/f| < 0$ (where S is the horizontal strain rate of the horizontal flow). Note that the first two singularity conditions coincide with the conditions for gravitational and centrifugal instability, respectively. The third singularity condition lies within the regime of moderate Rossby number, $0 < A/f < 1$, where AAI has been shown to occur.

In this paper we report a further test of the hypothesis that AAI is generic by examining a different flow regime, a barotropic boundary current with—as a modest generalization of the previous AAI examples—nonuniform shear and a quiescent far-field interior (Fig. 1) in a uniformly rotating, stratified fluid (i.e., constant f and N). Taken together, these examples of AAI are progressively coming closer to representing geophysically realistic types of background shear flows, although further steps remain (Sec. IV).

II. EIGENVALUE PROBLEM

We consider an incompressible, inviscid fluid dynamics expressed by the Boussinesq equations with a simple equation of state such that the density is conserved on material parcels. The background boundary current (Fig. 1) is a stationary solution of these equations, with the following particular, nondimensional profiles of velocity and buoyancy [where buoyancy is defined by $b = -g(\rho/\rho_o - 1)$, with g the gravitational acceleration, ρ the density, and ρ_o a constant reference density]:

$$V(x) = \mathcal{S}e^{-x} \quad \text{and} \quad B(z) = z. \tag{3}$$

There is an associated background pressure field in hydrostatic, geostrophic balance and no mean flow in the other directions (i.e., $U = W = 0$). Here (x, y, z) and (U, V, W) are coordinates and basic state velocities in the (cross stream,

downstream, upward) directions. The parameter $\mathcal{S}$ has the value $+1$ or -1 for anticyclonic or cyclonic background shear, respectively, when $f > 0$. Note that $\partial_x V$ has the same sign everywhere; this precludes an inflection-point instability for this flow. (To avoid having an inflection point, we have had to ignore a viscously supported boundary condition of no flow at the boundary $x = 0$; this limitation is further discussed in Sec. IV.) Note also that

$$A = f[1 - \mathcal{S} \operatorname{Ro} e^{-x}], \tag{4}$$

so the constraint that $0 \leq \operatorname{Ro} \leq 1$ assures centrifugal stability ($A/f > 0$). Gravitation instability is precluded by the positive background stratification, $\partial_z B = 1$.

The nondimensionalization for both the background state (3) and the Boussinesq equations below is based on the set of dimensional scales, $(\rho_o, V_o, H, L, f, N)$. V_o is the speed of the background current; L is the interiorward decay scale of the current; H is the domain height; and f and N are the Coriolis and Brünt-Väisällä frequencies. Given these primary scales, the following scales are used for nondimensionalization of the independent and dependent variables: horizontal length, L; vertical length, H; horizontal velocity, V_0; time scale, L/V_0; dynamic pressure, $p = \rho_o f V_0 L$; background buoyancy gradient, N^2; perturbation buoyancy, $f V_0 L/H$; and vertical velocity, $w = f V_0^2/N^2 H$. This nondimensionalization is consistent with quasigeostrophic asymptotics, and it is designed to expose the generally weak deviations of the flow from hydrostatic, gradient-wind diagnostic force balance when Ro and Fr are small.[11]

The nondimensional Boussinesq equations, linearized about the background state (3), govern the evolution of the small-amplitude perturbation fields, (u, v, w, p, b)

$$\operatorname{Ro}\left(\frac{\partial u}{\partial t} + V \frac{\partial u}{\partial y}\right) - v = -\frac{\partial p}{\partial x}, \tag{5}$$

$$\operatorname{Ro}\left(\frac{\partial v}{\partial t} + u \frac{\partial V}{\partial x} + V \frac{\partial v}{\partial y}\right) + u = -\frac{\partial p}{\partial y}, \tag{6}$$

$$\operatorname{Fr}^2 \lambda^2 \left(\frac{\partial w}{\partial t} + V \frac{\partial w}{\partial y}\right) = -\frac{\partial p}{\partial z} + b, \tag{7}$$

$$\frac{\partial u}{\partial x} + \frac{\partial v}{\partial y} + \frac{\operatorname{Fr}^2}{\operatorname{Ro}} \frac{\partial w}{\partial z} = 0, \tag{8}$$

$$\frac{\partial b}{\partial t} + V \frac{\partial b}{\partial y} + w = 0, \tag{9}$$

together with the boundary conditions, $w = 0$ at $z = 0$, 1. Here u, v, and w are cross-stream, stream-wise, and vertical perturbation velocity, and p and b are perturbation pressure and buoyancy. The nondimensional parameters that appear in (9) are the Rossby and Froude numbers defined in (1) and the aspect ratio, $\lambda = H/L$.

Normal modes are homogeneous solutions to (9). These eigenmodes have the separable functional form of, e.g.,

$$u(x,y,z,t) = \hat{u}(x)\cos[mz]e^{ily+\sigma t} + \text{c.c.}, \qquad (10)$$

where (m,l) are the (vertical, downstream) wave numbers, σ is the complex growth rate, and c.c. denotes the complex conjugate. The rigid vertical boundaries are at $z=0, 1$, where $w=0$. The analogous forms for (v,p) have a vertical factor $\cos[mz]$, while those for (w,b) have a factor $\sin[mz]$. The vertical boundary conditions are satisfied for the quantized values of $m=0, \pi, 2\pi, \ldots$. The resulting eigenvalue problem for the cross-stream functions is the following:

$$\text{Ro}(\sigma\hat{u} + ilV\hat{u}) - \hat{v} = -\partial_x\hat{p}, \qquad (11a)$$

$$\text{Ro}(\sigma\hat{v} + ilV\hat{v} + \partial_x V\hat{u}) + \hat{u} = -il\hat{p}, \qquad (11b)$$

$$\text{Fr}^2\lambda^2(\sigma\hat{w} + ilV\hat{w}) = m\hat{p} + \hat{b}, \qquad (11c)$$

$$\partial_x\hat{u} + il\hat{v} + \frac{\text{Fr}^2}{\text{Ro}}m\hat{w} = 0, \qquad (11d)$$

$$\sigma\hat{b} + ilV\hat{b} + \hat{w} = 0. \qquad (11e)$$

The lateral boundary conditions are $\hat{u}=0$ at $x=0$ and boundedness of all fields as $x\to\infty$. The latter condition is imposed as

$$\partial_x\hat{u} = ik\hat{u}, \quad x\to\infty, \qquad (12)$$

where k is the solution of the algebraic equation,

$$k^2 = -m^2\left(\frac{\text{Fr}}{\text{Ro}}\right)^2 \frac{\text{Ro}^2\sigma^2 + 1}{\lambda^2\text{Ro}^2\sigma^2 + 1} - l^2, \qquad (13)$$

with $\text{Im}[k]\geq 0$ for bounded far-field solutions and $\text{Re}[\sigma]>0$ for unstable ones. Equation (13) is recognizable as the dispersion relation for an inertia-gravity wave (with imaginary σ and reak k) or a boundary-trapped Kelvin wave (with both σ and k imaginary). Any eigensolution of the form (10) must satisfy this relation if it has a nonzero amplitude beyond where V decays to zero in the far-field interior.

The system of ordinary differential equations (11) is discretized using finite differences in the cross-stream direction. For small growth rates, a near singularity is encountered at the position of the so-called critical layer ($\sigma\approx -ilV$). This is the reason why a high spatial grid resolution is required to correctly resolve the desired unstable eigenmodes for small but finite growth rates. The most unstable modes for the illustrative parameters that we consider in this paper have a critical layer around $x=0.2$, which is fairly close to the boundary. To improve the resolution both at the position of the critical layer and near the boundary at $x=0$, we use a moderate degree of grid stretching in x. We define a uniform grid in a transformed cross-stream coordinate,

$$x^* = \beta(e^{\alpha x} - 1), \qquad (14)$$

where $\beta = x^*_{\max}/[\exp(\alpha x_{\max}) - 1]$ and $x_{\max}$ is the cross-stream width of the computational domain. For all results here the width of the computational domain is $x_{\max}=4$. Since the resulting matrix is sparse and we are only interested in the few, largest eigenvalues, we use a Krylov subspace method as in Molemaker, McWilliams, and Yavneh.[6] This allows us to use
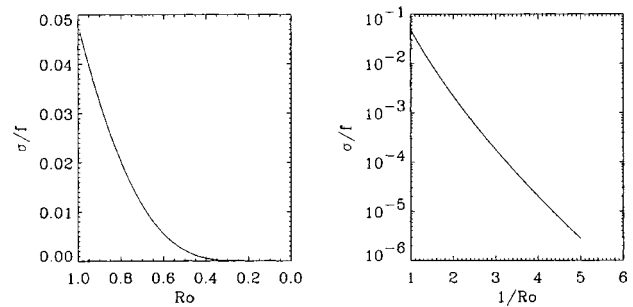

FIG. 2. Growth rate σ as a function of Ro, optimized over the vertical and horizontal wave numbers. $\mathcal{S}=1$ (anticyclonic background shear), Fr=Ro, and $\lambda=0.01$. The same function is plotted in different formats in the two panels.

very high spatial resolution where necessary, up to 8192 grid points in x^*.

III. UNSTABLE MODES

Apart from the wave number vector (l,m) and eigenvalue σ the eigenvalue problem (11) contains three independent parameters. Because of widespread experience that "Prandtl scaling," with $\lambda=H/L=f/N$, is usually approximately true for rotating, stratified fluid dynamics, we will make this choice for simplicity. It implies that Fr=Ro and reduces the independent parameters to λ and Ro. Should it turn out to be inappropriate for the AAI solutions here, this would become manifest in anomalous values of the most-unstable values of (l,m) that are internally defined by the eigenvalue problem. Also, since we will find that AAI is strongest for $m\gg 1$ (i.e., perturbation vertical scales much smaller than the domain height), we will usually view m as a continuous variable and ignore its finite-domain quantization.

We first calculate the growth rate of the most unstable mode as a function of Ro (Fig. 2). As in previously reported examples of AAI (Refs. 3–6), the growth rate decays approximately as an inverse-exponential function of decreasing $\text{Ro}>0$ [i.e., $\sim\exp(-c/\text{Ro})$ for $c>0$, a constant]. It does not exhibit a finite critical value in Ro below which there is no growth, but neither is it an algebraic function that might be obtained in a regular perturbation expansion about the quasi-geostrophic limit, $\text{Ro}\to 0$. In contrast, no unstable modes are found for a cyclonic background for $(\mathcal{S}=-1)$ and the comparable interval of $\text{Ro}<1$, as would be the default expectation for a stably stratified shear flow without either inflection-point or centrifugal instabilities allowed. This confirms the anticyclonic necessary condition for this instability type.

We broadly interpret these AAI modes as resonances where at least one inertia-gravity or Kelvin wave is involved. For an eigenmode problem like (11) with real-valued coefficients, any normal mode solution for a given (l,m) has an eigenvalue σ and eigenmode (u,v,w,p,b) such that there is another eigensolution with $-\sigma^*$ and $(-u^*,v^*,-w^*,p^*,b^*)$. If σ is purely imaginary (i.e., a neutrally stable mode), then this symmetry is a trivial one. But if $\text{Re}[\sigma]\neq 0$, then the symmetry is nontrivial, and it indicates that the modes occur in

$\pm |\mathrm{Re}[\sigma]|$ pairs with both exponentially growing (unstable) and decaying (damped) temporal behavior. Since the eigenmodes are countably finite in any spatial discretization of (11), then an instability that arises as a result of varying some control parameter (e.g., Ro) can only do so through the coalescence of the $\mathrm{Im}[\sigma]$ values for two neutral modes. This condition is sometimes called a resonance between two neutral modes.[12]

For a rotating stratified shear flow, the neutral modes occur in two classes that are well distinguished in particular limits. In the quasigeostrophic limit (Ro=0) for a flow without an inflection point, all the modes are neutral shear modes[2] with phase speeds lying within the speed range of $V(x)$. They have a continuous eigenvalue spectrum, and their spatial structure is singularly confined to the critical layer where $\mathrm{Im}[\sigma]=-lV(x)$. In the absence of a background flow ($V=0$) and nonzero f and N, all the modes with finite phase speed are inertia-gravity (spatially periodic) or Kelvin (boundary-trapped) modes, with phase speeds as specified from (13). In particular, for the configuration in Fig. 1 with $V=0$, the Kelvin-wave eigenmode with the form (10) is the following:

$$u = 0, \quad p = p_0 e^{-mx}, \quad v = -\frac{il}{\sigma \, \mathrm{Ro}} p,$$

$$w = m\sigma p, \quad b = -mp, \tag{15}$$

with $\sigma = il/m \, \mathrm{Ro}$.

In these respective limiting cases, the shear modes have a much slower propagation speed than the inertia-gravity modes by a factor $\mathcal{O}(\mathrm{Ro})$. Given that an instability occurring for finite Ro and V must be associated with a resonance of two neutral modes, our present interpretation is that one of each mode class is involved for AAI. In the case of stratified Taylor–Couette flow,[4,5] these are resonating shear-modified, boundary-trapped Kelvin waves, and for the baroclinic Eady flow,[6] an inertia-gravity wave and a shear mode are involved. Here, we suggest that a single shear-modified, boundary-trapped Kelvin wave resonates with a shear mode. The positive Doppler shift in the along-boundary phase speed due to the $V>0$ background flow approximately balances the negative Kelvin wave phase speed, $-\mathrm{Im}[\sigma]l<0$ implied by (13) for $\mathrm{Im}[k]>0$, to slow it down enough to coalesce with the $\mathcal{O}(\mathrm{Ro})$ slower phase speed of a shear mode. This coalescence by Doppler slowing of a cyclonically propagating Kelvin wave is only possible for anticyclonic background boundary currents (Fig. 1). So the absence of an instability for a cyclonic background current is consistent with this interpretation. On the other hand, given the singular character of the neutral shear modes, we do not believe it is feasible to track the modal coalescence to instability (cf. the tracking analysis in a two-layer flow by Sakai[12] where there is no neutral-mode critical layer).

To further support the implication of an inertia-gravity wave, we examine the dependence of the growth rate on N, for fixed Ro (Fig. 3) and the far-field structure of its associated eigenfunction. As also reported in the previous examples of AAI, the growth rate becomes constant for strong
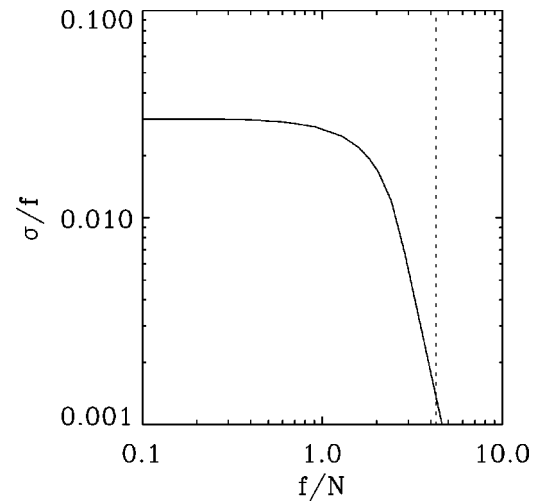

FIG. 3. Growth rate as a function of ratio of f/N, optimized over vertical and horizontal wave numbers. Ro=0.91 and $\mathcal{S}$=1. At values of f/N to the right of the vertical dashed line, the optimal vertical wavelengths, $2\pi/m$, exceed the depth of the domain.

stratification ($f/N \ll 1$), indicating the hydrostatic limit (Fig. 3). For weak stratification, the growth decays linearly with the stratification (i.e., $\propto N^2$ as $N^2 \to 0$), underscoring the importance of stratification, without which inertia-gravity waves could not exist. The value of the optimal vertical wave number is roughly constant with the parameter choice, $H/L = \lambda = f/N$. Thus, the vertical scale of the most unstable perturbation will be more than the total depth of the domain for weak stratification. This is the case for values of f/N larger than the value indicated with a vertical dotted line in Fig. 3, f/N=4.25. At this value of f/N, a half wavelength of the fastest growing mode spans the complete vertical extent of the domain with σ/f=0.0014. Along the path in parameter space for Fig. 3, the physical constants V_o, f, and L are unchanged while N^2 varies; thus, both Ro and Fr remain constant while $H = \lambda L = fL/N$ also varies.

In Fig. 4 the spatial patterns of the most unstable eigenmode components are shown for u, v, w, and p as horizontal slices at a level near the upper boundary. All fields have the largest amplitude near the boundary where the background horizontal shear is largest and the near-critical layer occurs (i.e., at $x \approx 0.16$). The location of the latter is most clearly evident in the downstream velocity perturbation v. This location is on the order of the Kelvin-wave boundary trapping scale in (15), viz., $m^{-1} \approx 0.08$. In the far field, all fields eventually decay in the cross-stream direction nearly as oscillatory, free inertia-gravity waves satisfying (13) for $\mathrm{Re}[\sigma]>0$ and $\mathrm{Im}[k]>0$.

For an unstable eigenmode with $\mathrm{Re}[\sigma]>0$, there is no singularity at the critical location, x_c defined by $\mathrm{Im}[\sigma] = -lV(x_c)$, since $|\sigma+ilV| \geq \mathrm{Re}[\sigma]>0$ and the corresponding coefficients in (11) do not vanish. For the mode in Fig. 4, $\mathrm{Re}[\sigma]$ is large enough that the near singularity in $v(x)$ is not particularly strong. However, when the instability is weaker (Fig. 5), the strength of the near singularity is greater. Nevertheless, for all the AAI modes that are the subject of this
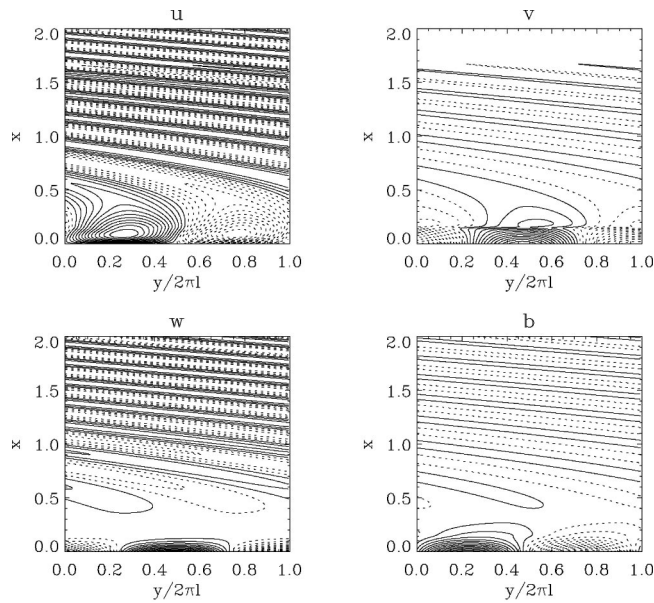
FIG. 4. Eigenmode horizontal structure for u, v, w, and p at $z=0.95$ for the most unstable perturbation for Ro=Fr=0.91 and $\lambda=0.01$, optimized over vertical and horizontal wave numbers (i.e., $l=3.7$ and $m=15$ for the largest Re$[\sigma]=0.03$; see Fig. 6). The maximum amplitudes of the fields, relative to $|u|_{max}=1.0$, are $|v|_{max}=2.5$, $|w|_{max}=2.7$, and $|b|_{max}=5.0$. The particular phase of the eigenmode is arbitrary since the problem has translation symmetry in the y direction.

paper, the eigenmode structure is well resolved by the computational grid defined by (14).

Figure 6 shows the wave number dependence of the AAI mode eigenvalue for the particular Ro=Fr and λ values. The instability expressed in Re$[\sigma]$ occurs over a broad range of wave numbers. It is favored for a nondimensional fluctuation aspect ratio l/m of about 0.25 relative to the Prandtl ratio of f/N implicit in the dimensionalizing aspect ratio. That is, AAI is favored for moderately flattened fluctuations compared to the ratio f/N that itself is typically small in nature. The instability is also favored for fluctuation downstream and vertical scales smaller than the unit horizontal scale of the background flow (i.e., $l,m\gg1$). The smallness of the
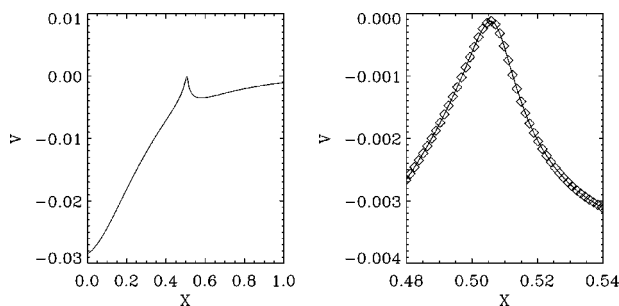

FIG. 5. Downstream-velocity eigenmode $v(x)$ for $t=0$, $y=\pi/2l$, $z=0.95$, $l=3$, $m=4$, Ro=Fr=0.91, and $\lambda=0.01$. For these parameters, $\sigma=0.01$. The near-critical layer is evident at $x\approx0.505$ on the left panel. A blow up of its neighborhood on the right panel shows that the near-singularity is computationally well resolved by the discrete grid points as plotted. This choice of (l,m) is nonoptimal (cf. Fig. 6) so that the relatively small growth rate value makes the eigenmode profile nearly singular.
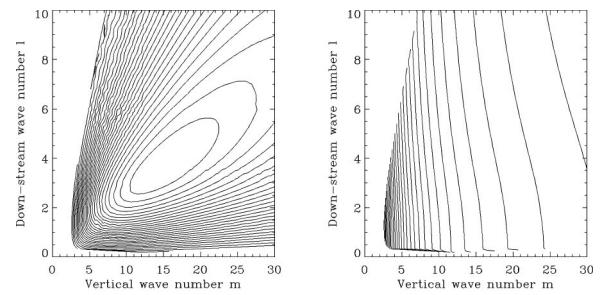

FIG. 6. Contour plot of growth rate (left) and phase speed (right) as functions of the horizontal and vertical wave numbers, l and m, for Ro=Fr =0.91 and $\lambda=0.01$. The contour levels are evenly spaced with a range of [0.0013, 0.030] for the growth rate and [0.32, 0.94] for the phase speed. Phase speeds are increasing for higher vertical wave number m.

fluctuation cross-stream scale is evident in the near-boundary confinement within $\Delta x\approx0.2$ in the particular eigenmode in Fig. 4.

Interpreting these modes as a resonant interaction of a wall bounded Kelvin wave with a shear mode we can use the phase speed $c_{ph}=$Im$(\sigma)/l$ of the unstable modes to infer the location of critical layer and the shear mode that makes up the resonant pair. Using the basic state velocity profile $V(x)=\exp(-x)$, the location of the critical layer can be found as $x_{cr}=-\ln(v_{ph})$. An example of this is the mode shown in Fig. 4, where the phase speed of the mode is $c_{ph}=0.85$. Modes with a lower phase speed are a result of interaction with a Kelvin wave further away from the boundary where its amplitude has decayed considerably. Consequently the resulting growth rate is much smaller.

The wave number dependence for the corresponding phase speed $c_{ph}=$Im$(\sigma)/l$ of the perturbation is shown in Fig. 6(b). It indicates that the phase speed increases for higher vertical wave numbers m. This corresponds to perturbation structures that are more trapped near the boundary.

We have additionally solved the modal instability problem for a variety of alternative stably stratified buoyancy and boundary-intensified, monotonically decaying current profile shapes in the same class as (3) (i.e., without an inflection point). The characteristics of the unstable AAI eigenmodes are robustly insensitive to the particular functional forms chosen. On the other hand, we have not presented modal solutions from flows with a horizontal inflection point. Our present understanding is that AAI has somewhat different behavior in this situation, and we intend to report about it later. (But recall that AAI in the Eady problem for baroclinic shear flow,[6] whose characteristics are consistent with those reported here, does have an inflection point associated with the vertical boundaries.)

IV. DISCUSSION

We have demonstrated another example of AAI in the context of a barotropic boundary current in an uniformly rotating and stratified fluid. By induction it seems likely that AAI is a generic behavior for strong anticyclonic flows. By induction from the available examples, we see that the characteristic dependences of the unstable growth rate on the rotation rate (inverse exponential decay as Ro$\rightarrow0$) and

stratification (linear decay as $N^2 \to 0$) are telltale indications of AAI. This behavior has been argued to be related to the spontaneous generation in stratified Couette flow of inertia-gravity waves whose amplitude decays exponentially with decreasing Rossby number.[13] From this behavior we infer that the third criterion for integrability of the balance equations, $A/f - |S/f| < 0$, does not indicate a sharp boundary for these instabilities, but rather it indicates a parametric neighborhood for the occurrence of AAI.

Given the Ro $\to 0$ asymptotic nature of the derivations of balanced equations and many similarly motivated, successful reductions of the primitive fluid dynamics (e.g., as surveyed in McWilliams and Gent,[14] and McWilliams[1]), this breakdown of diagnostic force balance at $\mathcal{O}(1)$ values of Ro and Fr with AAI—as with those associated with gravitational and centrifugal instabilities—is what should be expected for asymptotic consistency. None of these types of unbalanced instability can be derived by regular perturbation expansions in Ro, Fr about the quasigeostrophic limit (Ro, Fr $\to 0$) since their growth rate does not exhibit algebraic dependence on Ro.

Since successful diagnostic force balance models typically are nonunique at $\mathcal{O}(\text{Ro}^2, \text{Fr}^2)$, we can expect their integration singularities to be similarly nonunique. Thus, the occurrence of unbalanced instabilities may reasonably be associated with the neighborhoods of the singularity conditions, rather than precisely at these conditions. From this perspective the more puzzling question perhaps is why the onset instability behavior is so sharply confined to near the $N^2 = 0$ and $A = 0$ conditions for inviscid gravitational and centrifugal instabilities rather than why it is more broadly distributed around $A - |S| = 0$ for AAI. Perhaps it is because different diagnostic force balance models may show greater variety in their form of the third integrability condition than in forms of the first two conditions, but this conjecture cannot be tested until more such models have their integrability conditions explicitly identified. Nevertheless, it is evidently true that gravitational and centrifugal instability growth rates exhibit algebraic dependences on N/f and ζ/f beyond their respective critical values of 0 and 1; this is qualitatively different from the AAI inverse-exponential dependence as Ro $\to 0$.

If gravitational, centrifugal, Kelvin–Helmholtz, and AAI are indeed the generic instabilities of force-balanced flows, then the question arises of what will ensue once the unbalanced motions grow to finite amplitude. If their nonlinear advective dynamics *leads* to an efficient forward energy cascade to dissipation at small viscous scales, they may provide a more significant route to dissipation in the interior of the atmosphere and ocean than do the more energetic force-balanced flows since the paradigm for the latter is the inverse energy cascade of geostrophic turbulence.[15] These behaviors remain to be explored.

[1] J. C. McWilliams, in *Diagnostic Force Balance and its Limits*, Nonlinear Processes in Geophysical Fluid Dynamics, edited by O. U. Velasco Fuentes, J. Sheinbaum, and J. Ochoa (Kluwer Academic, Dordrecht, 2003), p. 287.

[2] P. G. Drazin and W. H. Reid, *Hydrodynamic Stability* (Cambridge University Press, Cambridge, 1981).

[3] J. C. McWilliams and I. Yavneh, "Fluctuation growth and instability associated with a singularity of the balance equations," Phys. Fluids **10**, 2587 (1998).

[4] M. J. Molemaker, J. C. McWilliams, and I. Yavneh, "Instability and equilibration of centrifugally-stable stratified Taylor–Couette flow," Phys. Rev. Lett. **86**, 5270 (2001).

[5] I. Yavneh, J. C. McWilliams, and M. J. Molemaker, "Nonaxisymmetric instability of centrifugally stable, stratified Taylor–Couette flow," J. Fluid Mech. **448**, 1 (2001).

[6] M. J. Molemaker, J. C. McWilliams, and I. Yavneh, "Baroclinic instability and loss of balance," J. Phys. Ocean. (submitted).

[7] T. Satomura, "An investigation of shear instability in a shallow water," J. Meteorol. Soc. Jpn. **59**, 148 (1981).

[8] T. Satomura, "An investigation of shear instability in a shallow water. Part II. Numerical experiment," J. Meteorol. Soc. Jpn. **60**, 227 (1982).

[9] R. W. Griffiths, P. D. Killworth, and M. E. Stern, "Ageostrophic instability of ocean currents," J. Fluid Mech. **117**, 343 (1982).

[10] J. C. McWilliams, I. Yavneh, M. J. P. Cullen, and P. R. Gent, "The breakdown of large-scale flows in rotating, stratified fluids," Phys. Fluids **10**, 3178 (1998).

[11] J. C. McWilliams, "A note on a uniformly valid model spanning the regimes of geostrophic and isotropic, stratified turbulence: Balanced turbulence," J. Atmos. Sci. **42**, 1773 (1985).

[12] S. Sakai, "Rossby–Kelvin instability: A new type of ageostrophic instability caused by a resonance between Rossby waves and gravity waves," J. Fluid Mech. **202**, 149 (1989).

[13] J. Vanneste and I. Yavneh, "Exponentially small inertia-gravity waves and the breakdown of quasigeostrophic balance," J. Atmos. Sci. **61**, 211 (2004).

[14] J. C. McWilliams and P. R. Gent, "Intermediate models of planetary circulations in the atmosphere and ocean," J. Atmos. Sci. **37**, 1657 (1980).

[15] J. G. Charney, "Geostrophic turbulence," J. Atmos. Sci. **28**, 1087 (1971).